MNRAS **439,** 2531–2541 (2014)
Advance Access publication 2014 February 7
doi:10.1093/mnras/stu112

The clustering of Galaxies in the SDSS-III Baryon Oscillation Spectroscopic Survey: including covariance matrix errors

Will J. Percival,[1⋆] Ashley J. Ross,[1] Ariel G. Sánchez,[2] Lado Samushia,[1,3] Angela Burden,[1] Robert Crittenden,[1] Antonio J. Cuesta,[4] Mariana Vargas Magana,[5] Marc Manera,[1] Florian Beutler,[6] Chia-Hsun Chuang,[7] Daniel J. Eisenstein,[8] Shirley Ho,[5] Cameron K. McBride,[8] Francesco Montesano,[2] Nikhil Padmanabhan,[2] Beth Reid,[6] Shun Saito,[6,9] Donald P. Schneider,[10,11] Hee-Jong Seo,[6] Rita Tojeiro[1] and Benjamin A. Weaver[12]

[1]*Institute of Cosmology and Gravitation, University of Portsmouth, Dennis Sciama Building, Portsmouth P01 3FX, UK*
[2]*Max-Planck-Institut fur Extraterrestrische Physik, Giessenbachstrae, D-85748 Garching, Germany*
[3]*National Abastumani Astrophysical Observatory, Ilia State University, 2A Kazbegi Ave., GE-1060 Tbilisi, Georgia*
[4]*Department of Physics, Yale University, 260 Whitney Ave, New Haven, CT 06520, USA*
[5]*Bruce and Astrid McWilliams Center for Cosmology, Department of Physics, Carnegie Mellon University, 5000 Forbes Ave, Pittsburgh, PA 15213, USA*
[6]*Lawrence Berkeley National Laboratory, One Cyclotron Road, Berkeley, CA 94720, USA*
[7]*Instituto de Fsica Teorica, (UAM/CSIC), Universidad Autonoma de Madrid, Cantoblanco, E-28049 Madrid, Spain*
[8]*Harvard–Smithsonian Center for Astrophysics, Harvard University, 60 Garden St, Cambridge, MA 02138, USA*
[9]*Kavli Institute for the Physics and Mathematics of the Universe (WPI), Todai Institutes for Advanced Study, The University of Tokyo, Chiba 277-8582, Japan*
[10]*Department of Astronomy and Astrophysics, The Pennsylvania State University, University Park, PA 16802, USA*
[11]*Institute for Gravitation and the Cosmos, The Pennsylvania State University, University Park, PA 16802, USA*
[12]*Center for Cosmology and Particle Physics, New York University, New York, NY 10003, USA*

Accepted 2014 January 15. Received 2013 December 18; in original form 2013 October 17

ABSTRACT

We present improved methodology for including covariance matrices in the error budget of Baryon Oscillation Spectroscopic Survey (BOSS) galaxy clustering measurements, revisiting Data Release 9 (DR9) analyses, and describing a method that is used in DR10/11 analyses presented in companion papers. The precise analysis method adopted is becoming increasingly important, due to the precision that BOSS can now reach: even using as many as 600 mock catalogues to estimate covariance of two-point clustering measurements can still lead to an increase in the errors of ∼20 per cent, depending on how the cosmological parameters of interest are measured. In this paper, we extend previous work on this contribution to the error budget, deriving formulae for errors measured by integrating over the likelihood, and to the distribution of recovered best-fitting parameters fitting the simulations also used to estimate the covariance matrix. Both are situations that previous analyses of BOSS have considered. We apply the formulae derived to baryon acoustic oscillation (BAO) and redshift-space distortion (RSD) measurements from BOSS in our companion papers. To further aid these analyses, we consider the optimum number of bins to use for two-point measurements using the monopole power spectrum or correlation function for BAO, and the monopole and quadrupole moments of the correlation function for anisotropic-BAO and RSD measurements.

Key words: cosmology: observations – distance scale – large-scale structure of Universe.

1 INTRODUCTION

With the increasing precision enabled by modern cosmological observations (e.g. Anderson et al. 2012; Planck Collaboration 2013), there is increasing interest in making their statistical analysis as rigorous as the measurements themselves. In this brief paper, we review the propagation of errors in the covariance matrix to the parameter errors, extending recent work (Taylor, Joachimi & Kitching 2012; Dodelson & Schneider 2013) to cover errors estimated by marginalizing over the likelihood recovered for each mock, and errors measured from the distribution of mocks that are also used to

⋆E-mail: will.percival@port.ac.uk

estimate the covariance matrix. These situations arose in our recent analysis measuring the baryon acoustic oscillation (BAO) position in the Baryon Oscillation Spectroscopic Survey (BOSS; Eisenstein et al. 2011; Dawson et al. 2013) Data Release 9 (DR9; Ahn et al. 2012) galaxy samples (Anderson et al. 2012), and in related analyses.

Many cosmological observations are well described as being drawn from a multivariate Gaussian distribution with inverse covariance matrix Ψ^t, where the superscript t denotes the true matrix, so that parameter inferences (such as finding the BAO position) can be based on a likelihood

$$\mathcal{L}(\boldsymbol{x}|\boldsymbol{p},\Psi^t) = \frac{|\Psi^t|}{\sqrt{2\pi}}\exp\left[-\frac{1}{2}\chi^2(\boldsymbol{x},\boldsymbol{p},\Psi^t)\right], \quad (1)$$

where

$$\chi^2(\boldsymbol{x},\boldsymbol{p},\Psi^t) \equiv \sum_{ij}\left[x_i^d - x_i(\boldsymbol{p})\right]\Psi_{ij}^t\left[x_j^d - x_j(\boldsymbol{p})\right]. \quad (2)$$

In the example of BAO fitting, the data $\boldsymbol{x}^d$, and model for the data $\boldsymbol{x}(\boldsymbol{p})$, would be power spectra or correlation functions, with the parameter $\boldsymbol{p}$ being the BAO position.

In many experiments, it is common to use mock, or simulated, data to estimate the inverse covariance matrix Ψ^t. Suppose we have n_b data measurements such as power spectrum band powers and wish to estimate the covariance matrix using n_s simulations. Assuming that the mock data can be written as x_i^s, with $1 \le i \le n_b$ and $1 \le s \le n_s$, the mean of each value over all simulations is

$$\mu_i = \frac{1}{n_s}\sum_s x_i^s, \quad (3)$$

and an unbiased estimate of the true covariance matrix $\mathbf{C}^t$ from these data is

$$C_{ij} = \frac{1}{n_s-1}\sum_s\left(x_i^s - \mu_i\right)\left(x_j^s - \mu_j\right). \quad (4)$$

The distribution of matrices recovered from multiple, independent sets of simulations follows the statistics of a Wishart distribution, and its inverse Ψ, from an inverse Wishart distribution with true inverse covariance matrix Ψ^t (e.g. Press 2005).

Because we do not know Ψ^t, we cannot use equation (1) directly, but should instead make parameter inferences using a joint likelihood

$$\mathcal{L}(\boldsymbol{x},\Psi|\boldsymbol{p},\Psi^t) = \mathcal{L}(\boldsymbol{x}|\boldsymbol{p},\Psi)\mathcal{L}(\Psi|\Psi^t), \quad (5)$$

where $\mathcal{L}(\Psi|\Psi^t)$ is given by an inverse Wishart distribution, while $\mathcal{L}(\boldsymbol{x}|\boldsymbol{p},\Psi)$ is the standard distribution given in equation (1), after replacing the true inverse covariance matrix with the estimate. We can subsequently marginalize over Ψ^t to obtain $\mathcal{L}(\boldsymbol{x},\Psi|\boldsymbol{p})$, which can be used to derive parameter measurements.

The marginalization over all elements in Ψ^t is computationally challenging; this limitation has led to an approximate approach, where the estimate of Ψ^t is used instead of the true inverse covariance matrix in equation (1), and the method and results from this approach are corrected. Marginalizing over the distribution of measured covariance matrices in equation (5) leads to two important corrections to this simplified approach.

(i) The inverse Wishart distribution has a form such that $\mathbf{C}^{-1}$, with $\mathbf{C}$ determined as in equation (4), is a biased estimate of the inverse covariance matrix.

(ii) The marginalization over possible true inverse covariance matrices increases the width of the error on any measured parameter from that recovered from $\mathcal{L}(\boldsymbol{x}|\boldsymbol{p},\Psi)$.

The first effect can be corrected by using an unbiased estimate of the inverse covariance matrix in the likelihood calculation

$$\Psi = (1-D)\mathbf{C}^{-1}, \quad D = \frac{n_b+1}{n_s-1}, \quad (6)$$

where the factor D accounts for the skewed nature of the inverse Wishart distribution (for the first cosmological application of this, see Hartlap, Simon & Schneider 2007).

Changing the covariance matrix in this manner does not correct for errors in the covariance matrix, which propagate through to errors on estimated parameters, so the second effect is still apparent. Suppose that the inverse covariance matrix estimate has an error $\Delta\Psi$ compared with the true matrix Ψ^t, with $\Psi = \Psi^t + \Delta\Psi$. For simulations drawn from a multivariate Gaussian, these errors can be calculated (Taylor et al. 2012),

$$\langle\Delta\Psi_{ij}\Delta\Psi_{i'j'}\rangle = A\Psi_{ij}\Psi_{i'j'} + B(\Psi_{ii'}\Psi_{jj'} + \Psi_{ij'}\Psi_{ji'}), \quad (7)$$

where

$$A = \frac{2}{(n_s-n_b-1)(n_s-n_b-4)},$$
$$B = \frac{(n_s-n_b-2)}{(n_s-n_b-1)(n_s-n_b-4)}. \quad (8)$$

In the following three sections, we consider how to use these error estimates to correct various parameter error calculations in order to fully account for the errors in the covariance matrix. In Section 2, we first follow the derivation of Dodelson & Schneider (2013), calculating the true error for measurements made from data that are independent from that used to estimate the covariance matrix. In Section 3, we consider how the covariance matrix errors propagate through to an estimate of the confidence interval derived from an individual likelihoods, and how measurements made from this approach must be corrected to give the true error. Section 4 considers the distribution of values recovered when fitting the same simulated data used to estimate the covariance: this exercise serves as a test of the method, allowing the full set of simulations to be used to both create and test the covariance matrix estimate. For consistency and brevity in these sections, we follow the notation of Dodelson & Schneider (2013) as closely as possible. The derived formulae are tested using Monte Carlo simulations in Section 5.

While following the propagation of errors in the covariance matrix through to parameter errors ensures that the estimated parameter errors are unbiased, this calculation does not mean that the corrected $\mathcal{L}(\boldsymbol{x}|\boldsymbol{p},\Psi)$ provides a maximum likelihood estimator for $\boldsymbol{p}$. Instead, the corrected parameter errors depend on the number of bins used when modelling the data, which can be considered as part of the methodology: smaller values of n_b give rise to less noisy estimates of the covariance matrix elements, while we cannot determine the elements of larger covariance matrices with the same precision. Using larger covariance matrices leads to increasingly large deviations in the accuracy of the parameter measurements compared with those that would have been made using the true likelihood. In Section 6, we provide a practical demonstration of the corrections, calculating the optimal number of bins to use when performing cosmological analyses of the latest BOSS galaxy clustering data.

2 THE COMBINED ERROR

Suppose that we have estimated the covariance matrix using a sample of simulations and wish to know the full error that we should expect on a measurement made using this covariance matrix and the

standard Gaussian likelihood, or equivalently the expected distribution of best-fitting parameter values that would be recovered from an independent set of simulations. This calculation was performed by Dodelson & Schneider (2013) and corresponds to determining the combined error on a measurement including both the data and covariance matrix errors.

We assume that the likelihood is calculated using the inverse covariance matrix estimate of equation (6). Following equation 24 of Dodelson & Schneider (2013), and using the standard summation convention, we can write the estimator for parameter p_α as

$$\hat{p}_\alpha = [F + \Delta F]^{-1}_{\alpha\alpha'} \frac{\partial x_i}{\partial p_{\alpha'}} \Psi_{ij} \left(x_j^d - x_j^t\right), \tag{9}$$

where F is the true Fisher matrix linearly relating the fitted parameter p to the measurements around the true likelihood peak

$$F_{\alpha\beta} \simeq \sum_{ij} \frac{\partial x_i}{\partial p_\alpha} \Psi^t_{ij} \frac{\partial x_j}{\partial p_\beta}, \tag{10}$$

and similarly for ΔF as a function of $\Delta\Psi$. Also following Dodelson & Schneider (2013), and without loss of generality, we assume that the true values of the parameters $p_\alpha = 0$.

Dodelson & Schneider (2013) expanded equation (9) to find the second-order (s.o.) contribution to the expected distribution of recovered values.

$$\langle p_\alpha p_\beta \rangle|_{\rm s.o.} = B(n_b - n_p) F^{-1}_{\alpha\beta}, \tag{11}$$

where B was given in equation (8), and n_p is the number of parameters measured. Thus, the corrected variance is

$$V_{\alpha\beta} = [1 + B(n_b - n_p)] F^{-1}_{\alpha\beta}. \tag{12}$$

This result, which was a key conclusion of Dodelson & Schneider (2013), describes the additional contribution to the data error from a covariance matrix calculated from simulations. It matches the distribution of best-fitting parameter measurements made from a set of simulations that is independent of those used to estimate the covariance matrix. However, this correction cannot be directly applied to an error derived from the likelihood derived from a particular mocks (as made in Anderson et al. 2012, for example), as is demonstrated in the next section.

3 ERRORS FROM THE LIKELIHOOD

In order to propagate the uncertainty in the covariance matrix through to errors estimated from the recovered likelihood for a particular fit, we first review how these errors are usually calculated. The best-fitting measurement can be made by integrating over the likelihood

$$\hat{p}_\alpha = \int \frac{p_\alpha}{\sqrt{2\pi|\Psi^{-1}|}} \exp -\frac{1}{2}\chi^2(\boldsymbol{x}, \boldsymbol{p}, \Psi)\, {\rm d}p, \tag{13}$$

with χ^2 defined as in equation (2). In the multivariate Gaussian approximation around the best-fitting solution, this expression reduces to equation (9).

The (squared) error on the measurement can also be estimated by integrating over the likelihood,

$$\hat{\sigma}^2_{\alpha\beta} = \int \frac{(p_\alpha - \hat{p}_\alpha)(p_\beta - \hat{p}_\beta)}{\sqrt{2\pi|\Psi^{-1}|}} \exp -\frac{1}{2}\chi^2(\boldsymbol{x}, \boldsymbol{p}, \Psi)\, {\rm d}p. \tag{14}$$

If Ψ were known perfectly (i.e. we replace Ψ with Ψ^t), equation (14) would recover a parameter variance of $[F]^{-1}_{\alpha\beta}$, from the definition of the Fisher matrix. The error in Ψ instead leads to a revised variance estimate

$$\hat{\sigma}^2_{\alpha\beta} = [F + \Delta F]^{-1}_{\alpha\beta}. \tag{15}$$

A Taylor series expansion then gives

$$\hat{\sigma}^2_{\alpha\beta} = F^{-1}_{\alpha\beta} + (F^{-1}\Delta F\, F^{-1}\Delta F\, F^{-1})_{\alpha\beta}, \tag{16}$$

ignoring first-order terms that will lead to zero expectation. Using the analogue of equation (10) for ΔF as a function of $\Delta\Psi$, and substituting in equation (7), we see that the error from the covariance matrix estimation increases the recovered variance to yield

$$\hat{\sigma}^2_{\alpha\beta} = [1 + A + B(n_p + 1)] F^{-1}_{\alpha\beta}. \tag{17}$$

Thus, the error in the covariance matrix has a biased effect on errors derived from the likelihood from any particular fit: on average they are larger than the errors would have been if we knew the true inverse covariance matrix. Unfortunately, the increase in size does not match the increase required to correct the distribution of best-fitting values recovered from independent data as derived by Dodelson & Schneider (2013), and presented in the previous section. To obtain an unbiased estimate of the full variance on parameter p_α, given a measurement of the error made using the standard method of integrating over the likelihood, we therefore must apply a factor of

$$m_1 = \frac{V_{\alpha\beta}}{\hat{\sigma}^2_{\alpha\beta}} = \frac{1 + B(n_b - n_p)}{1 + A + B(n_p + 1)} \tag{18}$$

to the measured parameter covariance, and the square root of this expression to the measured standard deviation.

Because the correction to the measured parameter covariance is independent of the value of the parameters around which the variance is measured, this correction should be applied even if we wish to estimate errors from the recovered likelihood, calculated by fitting to the same data used to estimate the covariance matrix.

4 DISTRIBUTION OF SAME DATA

In general, one wants to construct the best covariance matrix possible, in order to minimize the additional error. Thus, if this matrix is to be based on simulations, it is strongly desirable to use all available simulations. A classical approach is to apply any data analysis pipeline to mock data in order to test for any problems. If all mocks have already been used to estimate the covariance matrix, however, we should not expect to recover a distribution of best-fitting solutions that matches the equations derived in Section 2.

Consequently, it is worth examining how the expected error changes when we analyse the distribution of best-fitting values recovered from the same data set used to estimate the covariance matrix. In this case, we can write

$$\left\langle \left(x_i^d - x_i^t\right)\left(x_j^d - x_j^t\right)\right\rangle = (1 - D)(\Psi^{-1})_{ij}, \tag{19}$$

from equations (4) and (6). Substituting this equation into an expansion of $\langle p_\alpha p_\beta \rangle$, with p_α as in equation (9), we find

$$\langle p_\alpha p_\beta \rangle = (1 - D)[F + \Delta F]^{-1}_{\alpha\beta}. \tag{20}$$

Using the same approach that led from equation (15) to equation (17) yields

$$\langle p_\alpha p_\beta \rangle = \left[(1 - D)(1 + A + B(n_p + 1))\right] F^{-1}_{\alpha\beta}. \tag{21}$$

Therefore, the distribution of best-fitting parameter values recovered from data that were also used to estimate the covariance matrix is

biased in a different way to that of an independent set of data, and from the covariance estimate made from the measured likelihood. However, we can still use the recovered distribution to test the methodology provided we include the revised bias when analysing the result. Here, we need a corrective factor

$$m_2 = \frac{V_{\alpha\beta}}{\langle p_\alpha p_\beta \rangle} = (1 - D)^{-1} m_1, \tag{22}$$

with m_1 defined as in equation (18).

5 TESTING USING MONTE CARLO SIMULATIONS

In order to test the relative methods for determining errors, we have created Monte Carlo simulations for a model matching that of Dodelson & Schneider (2013). Here, we assume that each data vector comprised of n_b values is independently drawn from a standard Gaussian distribution (mean = 0, variance = 1) and that n_s of these data vectors are used to calculate a covariance matrix. The covariance matrix is allowed to include 'apparent' correlations between different data points, even though the true covariance matrix is diagonal. From any set of data, the parameter we wish to estimate is the average p_α, which has the expected value $E(p_\alpha) = 0$ and true variance $1/n_b$. The one-dimensional true Fisher matrix and its inverse are therefore $F_{\alpha\alpha} = n_b$, $F^{-1}_{\alpha\alpha} = 1/n_b$.

We have created 10^5 Monte Carlo *runs* for every n_b and n_s tested, averaging the measurements over all runs to provide our results. For each run, we created a set of n_s data vectors from which we calculated the covariance matrix and a set of n_s independent data vectors, which we used to test the fit. All of these data (both dependent and independent data sets) were fitted using the estimated covariance matrix, using equation (1) to estimate the likelihood. We therefore performed $2n_s$ likelihood fits for each run, finding the mean and variance as described in Section 3. Estimates of the variance derived in different ways from these fits are shown in Fig. 1. We do not apply any bias corrections to these data, but instead plot them as if they had been naively used to estimate the true variance.

The average variance of the distribution of best-fitting parameters recovered from the fits to the independent sets of data are shown by the open circles in Fig. 1 and are well matched to the formula derived by Dodelson & Schneider (2013, dot–dashed line, given by equation 12). These data represent the true error that should be quoted on measurements. The difference between these data and the solid line shows the extra variance introduced by the noisy covariance matrix estimate.

If we estimate the variance using the likelihood, or using the distribution of data also used to estimate the covariance matrix, we find a biased value. The average variance recovered by integrating over the likelihood as in equation (14) is plotted in Fig. 1 (solid circles) – the root of these values is commonly quoted as parameter errors in analyses. As described in Section 3, for parameters that linearly depend on the data (or in the standard approximation around the likelihood maxima), the best-fitting value around which we measure the variance does not matter. Thus, we recover exactly the same likelihood errors in our model whether we use the independent data or the data also used to estimate the covariance matrix. These estimates are biased and the offset is well matched to equation (17), which is indicated by the dashed line in the plots. The solid triangles show the variance estimated from the distribution of best-fitting values recovered from the same data set used to calculate the covariance matrix. These points are well matched to the dotted line,

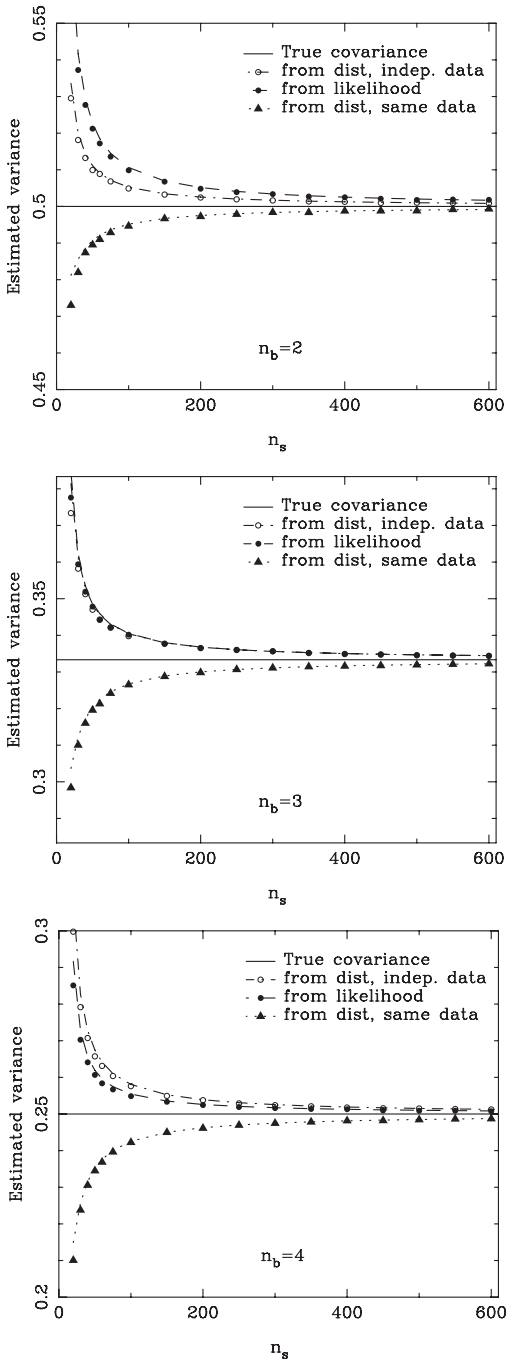

Figure 1. Estimated variance for the mean of n_b independent standard Gaussian random variables. The symbols show the estimated variance, averaged over 10^5 runs, each using n_s data vectors to calculate the covariance matrix. The solid circles show the average variance, calculated from the n_s likelihood-distribution-derived fitting to n_s independent data vectors (see Section 3), open circles from the distribution of best-fitting solutions recovered from these data (see Section 2), and the solid triangles from the distribution of best-fitting solutions when the same data used to estimate the covariance matrix is fitted (see Section 4). No corrections were applied to these estimates – i.e. we assumed that parameters A, B, or D were zero when making these variance estimates. The lines show the true data-only variance (solid), and the result after including the first-order theoretical corrections to the variance from the covariance matrix contribution (dot–dashed), the average variance estimated naively from the likelihood (dashed) and from the distribution of data values that were also used to calculate the covariance matrix (dotted).

calculated using the formula given in Section 4. As can be seen, this estimate of the variance is biased low, as a consequence of the offset between the estimated covariance and the inverse covariance matrix as given by the extra factor in m_2 compared with m_1.

In this plot, the factor m_1 is the ratio between the dashed and dot–dashed lines, and m_2 is the ratio between the dotted and dot–dashed lines. These factors correct these estimates to produce the true combined error (dot–dashed line) including both the standard variance and the effect of the noisy covariance matrix.

6 COSMOLOGICAL MEASUREMENTS WITH BOSS TWO-POINT STATISTICS

6.1 Estimating the covariance matrix from mocks

We now apply the calculations described above to investigate cosmological measurements made with the power spectrum and correlation function from BOSS. In this work, we focus on the CMASS galaxy sample, although our results could also be applied to the LOWZ sample. BOSS (Dawson et al. 2013) is part of the Sloan Digital Sky Survey-III (SDSS-III; Eisenstein et al. 2011) project, which used the SDSS telescope (Gunn et al. 2006) to obtain imaging (Gunn et al. 1998) and spectroscopic (Smee et al. 2013) data, which was then reduced (Bolton et al. 2012) to provide a sample of galaxy redshifts, with known mask. We focus on the BAO methodology described in Anderson et al. (2012, 2013) and Anderson et al. (2013b) and the redshift-space distortion (RSD) methodology of Reid et al. (2012) and Samushia et al. (2013).

In Anderson et al. (2012) and Reid et al. (2012), we used 600 PTHaloe mock catalogues to analyse the BOSS DR9 sample, both to understand the analysis methodology and to determine covariance matrices for the two-point measurements. These mock catalogues were created as described in Manera et al. (2013). Briefly, 600 second-order Lagrangian perturbation theory (2LPT) matter fields were created in boxes of size $L = 2400\,h^{-1}$ Mpc, sampled by 1280^3 dark matter particles. Within these boxes, haloes were found with a friends-of-friends group finder (Davis et al. 1985) with appropriate linking length, and their masses were calibrated by detailed comparisons with N-body simulations. The haloes were populated with mock galaxies using a halo occupation distribution (Peacock & Smith 2000; Berlind & Weinberg 2002; Cooray & Sheth 2002) prescription, which was calibrated to reproduce the clustering measurements on scales between 30 and $80\,h^{-1}$ Mpc. Mock catalogues were then created by sampling these boxes to match the geometry and efficiency of the project. Mock catalogues have also been drawn from these boxes for the DR10 (Ahn et al. 2013) and DR11 samples used in Anderson et al. (2013b) to measure the BAO positions (Manera et al. 2013).

In order to create the mocks, we treat the northern Galactic cap (NGC) and southern Galactic cap (SGC) components of the survey as being independent and sample them separately from the same set of boxes. For the DR9 analysis, we could easily sample the north and south components of the survey from the 600 boxes without overlap, giving 600 NGC mocks and 600 SGC mocks that are independent. Given the volume covered by the DR10 and DR11 BOSS CMASS galaxy samples, we could not easily sample both parts of the survey from each box without overlap, meaning that the NGC and SGC mocks drawn from the same box are not independent. To construct joint NGC+SGC mocks, we sample the NGC from one subset of 300 simulations and combine these with samples of the SGC from the remaining independent simulations. An equivalent set of combined mocks can be created by instead sampling the SGC from the first subset of 300 simulations and the NGC from the remaining 300 simulations. While both of these sets should provide unbiased estimates of the covariance matrix, they are in principle correlated with each other, as the set of NGC mocks used to calculate one is correlated with the set of SGC mocks used to calculate the other. We then estimate the covariance matrix for the joint NGC+SGC power spectrum as the average from these two, each calculated from 300 (NGC+SGC) mock power spectra. The final equation for our covariance matrix is

$$2\hat{C}_{ij} = \frac{1}{299}\sum_{m<300}[P_i^m(k)-\bar{P}_i(k)][P_j^m(k)-\bar{P}_j(k)] + \frac{1}{299}\sum_{m>300}[P_i^m(k)-\bar{P}_i(k)][P_j^m(k)-\bar{P}_j(k)], \quad (23)$$

where $P_i^m(k)$ is the measured power spectrum from mock m in bin i, and $\bar{P}_i(k)$ is the mean calculated separately for each set of 300 mocks. A similar equation is used to calculate the covariance matrix for the correlation function. Although this approach produces an unbiased estimate of the covariance matrix, the two contributions are correlated, so the sum would not produce the $\sqrt{2}$ reduction in noise in the covariance matrix as would be expected for the combination of independent estimates, if we could approximate components as being Gaussian.

Table 1. The effective areas of the DR9, DR10, and DR11 BOSS CMASS galaxy samples, and the overlap areas when mocks are sampled from the same parent box. r is the correlation coefficient between estimators, and $(1 + r^2)/2$ reflects the reduction of the covariance errors when the estimators are combined.

Sample	Area (deg^2)			r	$(1 + r^2)/2$
	NGC	SGC	Overlap		
DR9	2584	690	28	0.016	0.50
DR10	4817	1345	1006	0.33	0.55
DR11	6308	2069	2069	0.49	0.62

In fact, for DR9, when projected into the mock boxes, the NGC and SGC components of the survey only have a small overlap and we were therefore justified in treating both sets of mocks as independent. However, for DR10, the overlap is approximately 75 per cent of the area covered by the SGC, while for DR11, the entire southern component is also covered by the NGC (see Table 1). If we assume that the variance on the measurement is proportional to the inverse of the effective volume $V_{\rm eff}$, the correlation coefficient between (NGC+SGC) mock measurements with overlapping NGC and SGC components, so that the NGC for one overlaps with the SGC of the other, and vice-versa, is given by $r = 2V_{\rm overlap}/(V_{\rm NGC} + V_{\rm SGC})$. The degree of overlap above results in $r = 0.33$ for DR10 and $r = 0.49$ for DR11. Again, to be explicit, this correlation coefficient represents how strongly the power spectrum error in one mock correlates with that in another mock, where the two mocks sample either NCG+SCG or SGC+NGC from two simulations.

Ultimately, we are interested in how these correlations impact the covariance error resulting from the combined estimator of equation (23), compared to the covariance error which arises from using a single set of 300 mock catalogues. We find that the power spectrum correlation propagates into the combined covariance error, which we effectively model by rescaling the error terms given by A, B and D in equations (8) and (6) by a factor of $(1 + r^2)/2$, which is that standard formula for the variance of the average of two correlated random variables. In the limit of large n_s, the B term dominates

over the A term in equation (8); this is equivalent to rescaling the number of simulations by a factor of $2/(1 + r^2)$. Thus, for DR9, where the correlations are negligible, the effect is simply to increase the effective number of simulations by a factor of 2, as one might expect.

6.2 Application to DR9 BAO measurements

Error bars for the BAO measurements presented in Anderson et al. (2012) were derived from the likelihood calculated from fitting either the isotropically averaged power spectrum or correlation function with a model that marginalizes out the broad-band components of the two-point functions, leaving the BAO whose scale can be measured. For the power spectrum analysis of Anderson et al. (2012), we fitted 70 band powers with a model including 11 parameters, and neither the correction shown in equation (6) nor the factor in equation (18) were applied to the inverse covariance matrix. Both the factors are of the order of 10 per cent and act to increase the size of the variance from the raw value measured. The quoted errors on the power spectrum-based BAO position measurements provided in Anderson et al. (2012) should therefore be increased by 12 per cent given the current analysis: i.e. post-reconstruction, we quoted $\alpha = 1.042 \pm 0.016$, but these will change with the current error analysis to $\alpha = 1.042 \pm 0.018$.

For the correlation function analysis of Anderson et al. (2012), we fitted 44 binned points $28 < r < 200\,h^{-1}$ Mpc, using a model with five free parameters. As with the fits based on the power spectrum, error bars were derived from the likelihood, and neither the correction to the inverse covariance matrix estimate (equation 6) nor the correction because of the error in the covariance matrix (equation 18) were applied. Because of the reduced number of bins and degrees of freedom, the corrections are slightly smaller than in the power spectrum case, and are of the order of 4 and 3 per cent, respectively, for the error. The errors on the correlation function-based BAO position measurements provided in Anderson et al. (2012) would therefore need to be increased by 7 per cent given the current analysis: i.e. post-reconstruction, Anderson et al. (2012) quoted $\alpha = 1.024 \pm 0.016$, but these values will change with the current error analysis to $\alpha = 1.024 \pm 0.017$.

6.3 Application to DR10 and DR11 monopole power spectrum BAO measurements

The default BOSS DR10 analysis presented in Anderson et al. (2013b) uses 600 mocks, calculated as for DR9, but with an updated angular mask. We have measured the power spectrum for each of these mocks after reconstruction, using the standard pipeline described in Anderson et al. (2012). Each power spectrum was binned into a large number of fine bins, which were then combined to produce results for various numbers of bins within the range of scales fitted $0.02 < k < 0.3\,h^{-1}$ Mpc. For each binning choice, we have estimated the covariance matrix, and window function, and used these to fit the data with a model given by

$$P^{\rm fit}(k) = P^{\rm sm}(k)[1 + (O^{\rm lin}(k/\alpha) - 1)e^{-\frac{1}{2}k^2\Sigma_{nl}^2}], \quad (24)$$

where the BAO scale α and the damping Σ_{nl} are parameters, and $P^{sm}(k)$ is a smooth model for the broad-band shape of the power spectrum, and $O^{\rm lin}(k)$ are the BAO extracted from the linear power spectrum $P^{\rm lin}(k) = O^{\rm lin}(k)P_{\rm sm,lin}(k)$. We have changed the fitting method from that in Anderson et al. (2012) in two key ways:

(i) we fit band powers in $\log P(k)$, which was shown to be close to having a multivariate Gaussian distribution in Ross et al. (2013), as expected in the sample-variance limited regime.

(ii) we use a model for the broad-band power spectrum

$$P^{\rm sm}(k) = B_p^2 P(k)^{\rm sm,lin} + A_1 k + A_2 + \frac{A_3}{k} + \frac{A_4}{k^2} + \frac{A_5}{k^3}, \quad (25)$$

which is better matched to that used for the correlation function than the $P(k)$ model used in Anderson et al. (2012). Our final model has six 'nuisance' parameters, B_p, A_1, A_2, A_3, A_4, and A_5; see Anderson et al. (2013b) and Ross et al. (2014) for further discussion of this issue.

For each mock, we have determined the best-fitting value of α and σ_α^2 by marginalizing over the other parameters using the derived likelihood. In this calculation, we assumed a Gaussian prior on Σ_{nl} of ± 2 centred on the best-fitting values determined by fitting the average recovered power spectrum. In principle, the BOSS data alone can measure this parameter simultaneously with the BAO scale measurement, albeit at the expense of an increase in the error. In fact, we have a strong prior from theory about the amplitude of this damping, which we include to reduce the impact on the BAO scale error (for more details see Anderson et al., in preparation).

We need to apply the corrections determined in Section 3 to the errors derived from the likelihood and, as the covariance matrix was also calculated from the same mocks used to determine the covariance matrix, the correction of Section 4 to the distribution of best-fitting values. The resulting measurements of the expected error on α are shown in Fig. 2 as a function of the number of bins in the fitted range $0.02 < k < 0.3\,h\,{\rm Mpc}^{-1}$. The upper sets of points and lines represent pre-reconstruction, with the lower set, corresponding to the more accurate fits, representing post-reconstruction.

The raw errors from these calculations are shown as the open (from the likelihood) and solid (from the distribution) circles, with the results after correction represented by the lines. The lower panel presents the percentage deviation of the mean, calculated from all of the mocks for different numbers of bins. This represents a systematic error on the recovered value of α.

From Fig. 2, we see that, after correction, the values of the errors recovered from the distribution and from the likelihood agree to a higher degree than before correction, particularly for small values of the bin width. There is an error on this match that results from the error in the covariance matrix, with the data from different bin widths being highly correlated. We expect this error to be of the same order as the difference between the corrections applied to the likelihood- and distribution-based errors as this difference results from the offset within the Wishart distribution from which the covariance matrix is derived (see Section 1). It therefore gives a crude estimate for the width of this distribution. This reasoning shows that the differences between corrected errors derived in the different ways are consistent.

Without correction, the statistical errors recovered from both methods decrease with increasing bin width, naively suggesting that increasing the number of bins increases the information content. In fact, the post-correction errors increase for small bin widths, demonstrating that we are simply transferring data noise into covariance matrix noise as we increase the number of bins, which is not appearing in the raw error calculation. After correction, the recovered errors are reassuringly independent of bin width for a wide range of bin widths. For small numbers of bins, the mean offset measured in the BAO location is small compared with the statistical errors, and is of the order of 0.4 per cent for the pre-reconstruction fits, while it is consistent with zero post-reconstruction, with an error

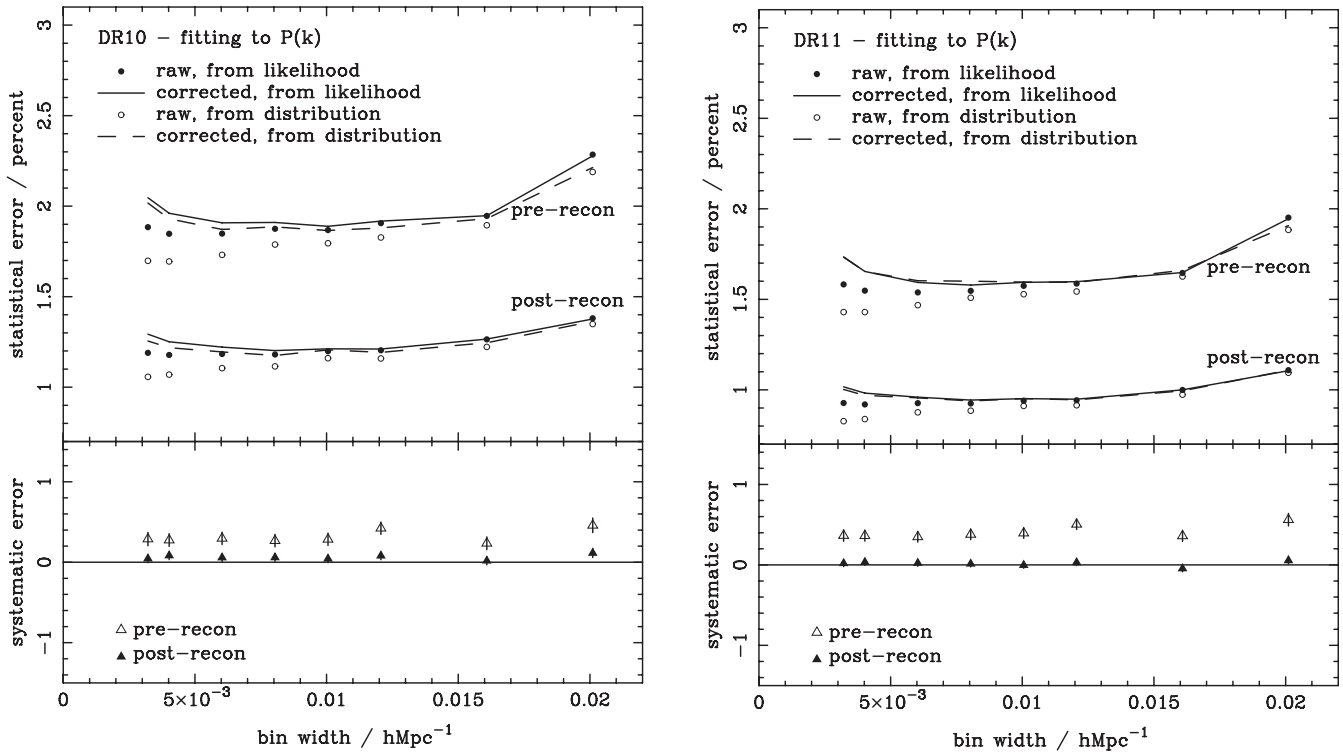

Figure 2. Top panels: recovered errors from the best-fitting values of α calculated by fitting the BAO as described in Anderson et al. (2012), but for the BOSS DR10 (left) and DR11 (right) mock samples (Manera et al. 2014). The solid circles and the solid line were determined from the likelihood, as described in Section 3, while open circles and the dashed line were calculated from the distribution of values recovered from the mocks as described in Section 4. The points represent the 'raw', uncorrected values, while the lines show the values after correcting for the covariance matrix. Lower panel: percentage error on the mean value of α recovered from the mocks.

of 0.04 per cent for all bin widths. The size of the systematic offset is not dependent on the bin width, giving us confidence that we are correctly modelling the binning effects. The low amplitude of the systematic errors post-reconstruction strongly suggests that we do not have any systematic biases due to the survey mask, our modelling of the resulting window function, or effects from the galaxy bias as implemented within the PTHaloes methodology (Manera et al. 2013).

Comparing both the offset in the mean value recovered and the recovered errors indicates that the optimum number of bins for the power spectrum analysis over $0.02 < k < 0.3\,h\,\mathrm{Mpc}^{-1}$ is approximately 35 with bin width $0.008\,h\,\mathrm{Mpc}^{-1}$, half the number of bins used in the DR9 analysis of Anderson et al. (2012). For such a small number of bins, the corrections required for the derived errors are small: equation (18) suggests that the likelihood derived errors need to increase by $\sqrt{m_1} \sim 3$ per cent.

6.4 Application to DR10 and DR11 monopole correlation function BAO measurements

We have performed a similar analysis to determine the optimum bin size for the BAO fits to the isotropic correlation function. Following the methodology adopted for Anderson et al. (2013b), we fix the BAO damping scale, leaving a five-parameter model composed of α and a four-parameter broad-band model that is similar to that described for the power spectrum in the previous section,

$$\xi^{\mathrm{fit}}(s) = B_\xi^2 \xi^{\mathrm{mod}}(\alpha s) + \frac{a_1}{s^2} + \frac{a_2}{s} + a_3. \quad (26)$$

Here, ξ^{mod} is the Fourier transform of a linear model for the correlation function with damped BAO (see Anderson et al. 2013b for more details), and a_i with $(1 < i < 3)$ are free parameters that marginalize over the broad-band signal. Because the BAO signal in the correlation function does not extend to non-linear scales to the same extent as in the power spectrum, the broad-band model can be added to the linear correlation function, which includes the BAO signal, rather than multiplying the BAO as in the $P(k)$ model (equation 24). This leaves a correlation function model with more freedom to dampen the BAO. Thus, for our correlation function fits, we fix Σ_{nl}^2 rather than including it as a free parameter with a Gaussian prior as for the power spectrum. The consequences of this difference are discussed further in Anderson et al. (2013b).

As for the power spectrum, we have fitted all 600 mocks using this model to determine a likelihood distribution for each. From this exercise, we have derived best-fitting values and expected errors on α, marginalizing over other parameters. We have also estimated the width of the distribution of recovered best-fitting values, taking care to produce an unbiased estimate by splitting the mocks into two sets of 300 independent measurements. The resulting errors, plotted as a function of number of bins, are shown in Fig. 3. The difference between results from the likelihood and the distribution are similar to those for the power spectrum fits. The size of these discrepancies are similar to the correction applied and as such may simply be a statistical deviation within the expected distribution. The results from different bin choices are obviously correlated to a high degree. We do not attempt to estimate the error on the correction that we are applying to the error – i.e. the error on the error on the error.

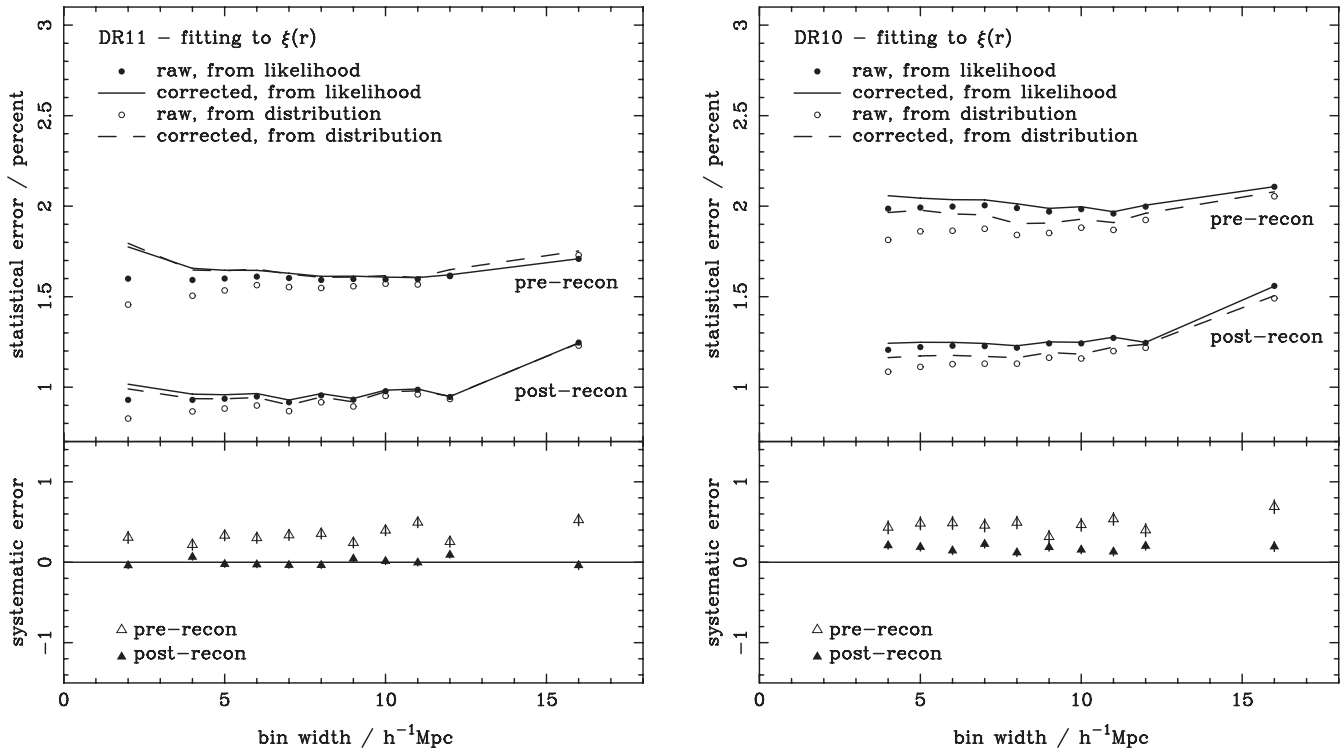

Figure 3. As Fig. 2, but now for the fits to the correlation function.

Fig. 3 reveals a flat minimum, with bins of width 6–10 h^{-1} Mpc all providing similar final errors on the BAO scale. We therefore recommend that the monopole of the correlation function, when fitted independently, be binned with width 8 h^{-1} Mpc. There is no evidence that binning on these scales induces a systematic error due to the coarseness of the averaging.

6.5 Application to DR11 anisotropic BAO measurements

We have also considered fits to the monopole and quadrupole moments of the correlation function using the methodology applied in Anderson et al. (2013a) and Anderson et al. (2013b). For simplicity we only present results from the DR11 data, although similar results are produced for DR10. Additionally, similar results are observed for fits to 'Wedges': top-hat averages of the anisotropic correlation function in the cosine of the angle to the line of sight (for more information see Kazin et al. 2013).

Fig. 4 presents the average errors on $\alpha_\perp$ and $\alpha_\parallel$ from the fits to the 600 mocks as a function of bin size. As in Fig. 2, these errors are shown with and without the correction factors for the error in the covariance matrix. The behaviour of the fits in the anisotropic case is quite similar to those from just fitting the monopole of the correlation function (Fig. 3). The minimum is quite broad, just pushing to slightly larger bin sizes than the monopole-only fits. Given our preference, for simplicity, we adopt a bin size of 8 h^{-1} Mpc for fits to both monopole only or monopole and quadrupole, rather than using a different bin for the two measurements.

The likelihood-based and distribution-based results are well matched after correcting for the covariance matrix effects, as for the monopole-only fits. There is some evidence for a small ∼0.5 per cent systematic offset on $\alpha_\parallel$, which was also seen in Anderson et al. (2013a). There is also evidence for 'oscillatory behaviour' of the errors as a function of bin width, which is particularly apparent for the post-reconstruction fits. For our binning scheme, as we increase the bin width, we also alter the positions of the bin centres. The ability to fit the position of the BAO is very sensitive to the bin centre for bins that cover the BAO signal and are large compared to that signal. This leads to variations in the recovered errors as seen. We also see an increase in the systematic offset for large bins, which is coupled to this lack of resolution. Clearly, it is desirable that this region is avoided.

6.6 Application to DR11 RSD measurements

We now extend the analysis to consider RSD measurements made from joint fits to the monopole and quadrupole moments of the correlation function. We limit the analysis to have the same bin width for both and consider how this choice affects the error on the final measurement. For this analysis, we have three free parameters.

(i) The amplitude of the real-space galaxy power spectrum, quantified by $b(0.57)\sigma_8(0.57)$, where $\sigma_8(z)$ is the root-mean-square amplitude of overdensity fluctuations in spheres of radius 8 h^{-1} Mpc.

(ii) The amplitude of the velocity field, which controls the RSD amplitude and is quantified by

$$f(0.57)\sigma_8(0.57) = \sigma_8(0)\left.\frac{\mathrm{d}G}{\mathrm{d}\ln a}\right|_{z=0.57}, \quad (27)$$

where $G(z)$ is the linear growth rate.

(iii) The width of the Gaussian probability distribution function assumed to model the non-linear Fingers of God, $\sigma_{\rm FOG}$.

Further details about these parameters can be found in Samushia et al. (2013). For speed, given the number of fits to be performed, unlike in Samushia et al. (2013), we do not allow the shape of the real-space power spectrum or the two dilation parameters $\alpha_\parallel$ and $\alpha_\perp$ that control the radial and angular projections to vary and fix

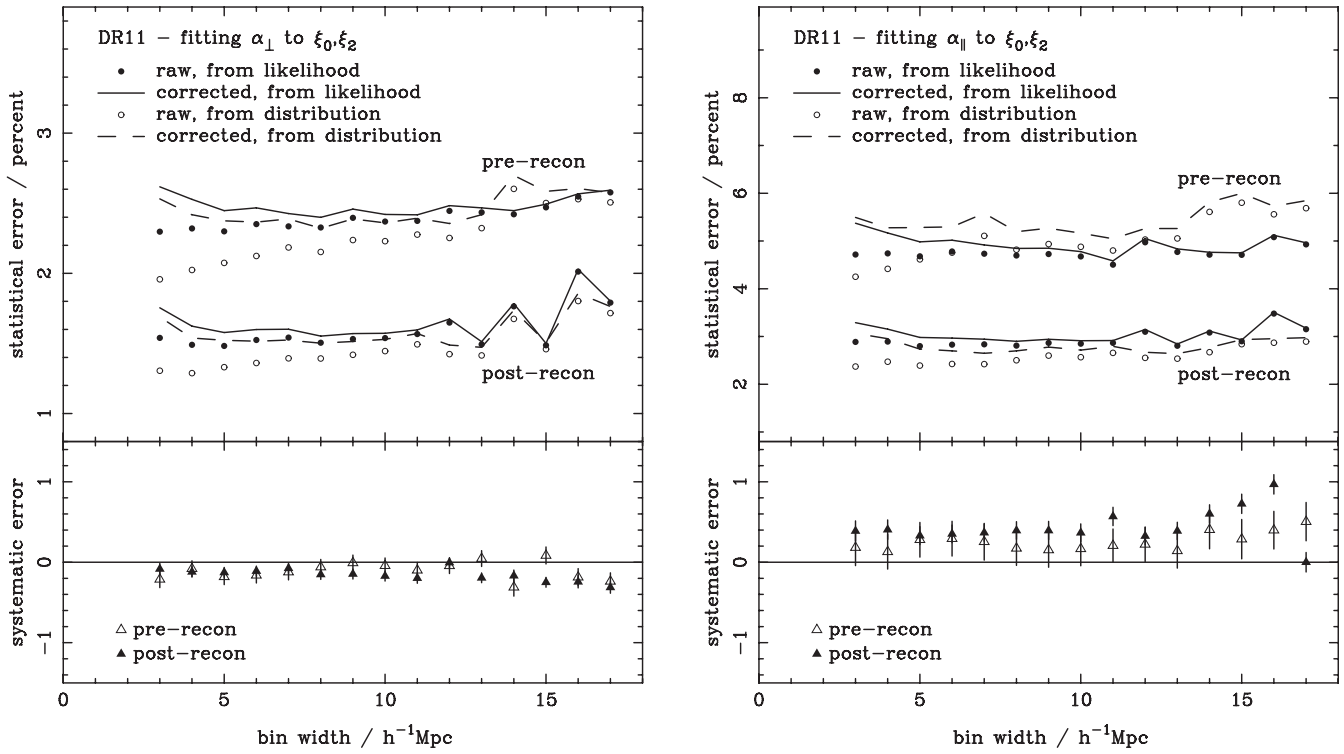

Figure 4. As Fig. 2, but now for BAO fits to monopole and quadrupole moments of the correlation function as described in Anderson et al. (2013b), now allowing for a different dilation of scale in the radial ($\alpha_\parallel$) and angular ($\alpha_\perp$) directions.

them at their true values. We do not expect this decision to alter our conclusions significantly given that this shape is highly constrained by the recent Planck results (Planck Collaboration 2013).

The results of our fits can be seen in Fig. 5, where we compare the standard deviations of the distribution of recovered values of $f\sigma_8$ against bin width. For each fit, we do not attempt to map the full likelihood, but instead use a minimization routine to find the maximum of the likelihood in parameter space. Thus, we only present results from the distribution of recovered best-fitting values. Given the similarity between results derived from individual likelihood distributions, and from the distributions presented in Sections 6.3 and 6.4, we believe that this approach is sufficient to determine the best bin width.

As can be seen in Fig. 5, for narrow bin width where large numbers of bins are used in the covariance matrix, there is an increase in the corrected error as for the BAO fits. There is no increase to large bin widths because the RSD measurement is effectively an amplitude determination unlike BAO fitting, which is a centroiding problem, and therefore large bin widths are more detrimental. Thus, RSD measurements are less sensitive to the bin width chosen. Most RSD determinations (e.g. Reid et al. 2012) perform a joint fit including the shape of the two-point measurement, and therefore the best-fitting BAO bin width of $\sim 8\,h^{-1}$ Mpc remains an optimal choice. The systematic errors shown in the lower panel of Fig. 5 are relatively large compared with those from BAO measurements. The large errors are partially due to the 2LPT mocks not reproducing the non-linear evolution of the growth rate exactly. The systematic offset would decrease if we fitted a 2LPT model to the measurements instead of the non-linear streaming model, which is more accurate for the data (see Samushia et al. 2013 for more details).

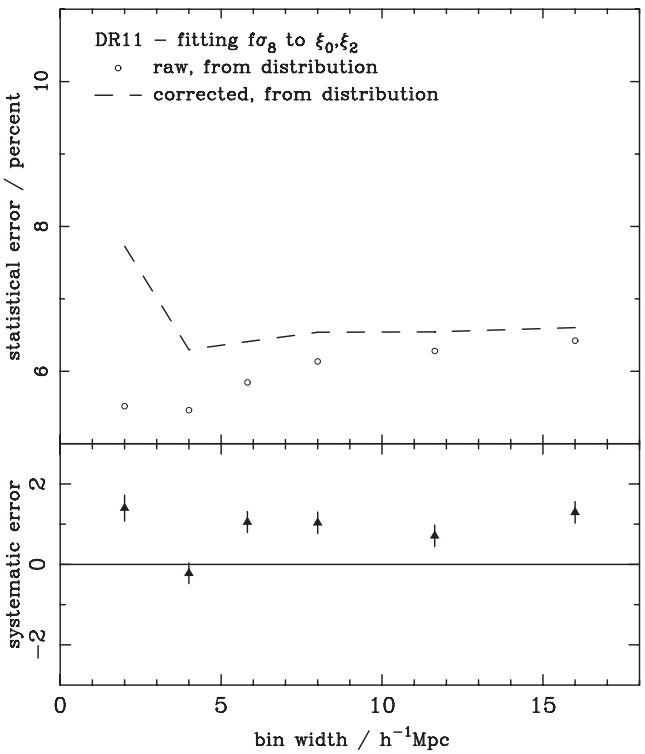

Figure 5. As Fig. 2, but now for RSD fits to monopole and quadrupole moments of the correlation function as described in Samushia et al. (2013).

7 DISCUSSION

In this paper, we have reviewed the calculations being performed using the latest BOSS data in order to extract cosmological measurements. Building upon a series of recent papers examining the errors in the inverse covariance matrix used in cosmological applications (Hartlap et al. 2007; Taylor et al. 2012; Dodelson & Schneider 2013), we have had to derive and understand the effect of two further errors in two further situations – where the error on final parameters is calculated by integrating over the derived likelihood and, in order to test the method, the distribution of best-fitting values recovered from the same set of mocks used to determine the covariance matrix. These derivations have been tested and shown to be accurate using Monte Carlo simulations.

To summarize, there are two corrections that must be applied to the 'naive' analysis simply inverting the covariance matrix derived from equation (4) and using it in equations (1) and (2). First, as pointed out by Hartlap et al. (2007), we must correct for the offset nature of the inverse Wishart distribution by correcting the inverse covariance matrix by the factor given in equation (6). Secondly, we need to correct for the additional contribution of the error in the covariance matrix to the final error on a derived parameter. Three different corrections to create unbiased error estimates exist in different situations.

(i) If the variance of a measurement is estimated from the distribution of best-fitting values recovered from data that are independent of that used to estimate the covariance matrix, the variance on the result is given in equation (12) (Dodelson & Schneider 2013). This variance corresponds to the true error on measurement from data (which are independent from the mocks used to calculate the covariance matrix).

(ii) If the variance is measured from a likelihood, calculated from fitting to a set of data (be it from independent mocks, the same mocks used to estimate the covariance matrix, or the actual data), we derive a biased estimate of the variance, which is different from the expression given by equation (12). To correct this bias, we must apply the correction m_1, given in equation (18), to the derived estimate.

(iii) If the variance is derived from the distribution of best-fitting values recovered from the same data also used to estimate the covariance matrix, we also obtain a biased result and must now apply the factor m_2 given in equation (22) to the estimate.

We have considered how the mocks used to determine the covariances for BOSS affect parameter inferences and have shown how they must be carefully analysed in order to take into account how they were produced, in particular the overlap between NGC and SGC components. Having done this, we have not only included the extra errors in our final measurement errors given in companion papers (Anderson et al. 2013b; Beutler et al. 2013; Chuang et al. 2013; Samushia et al. 2013; Sanchez et al. 2013; Tojeiro et al. 2014), but also used the derivation to understand the effect of bin size on the final errors. We have derived optimal binning strategies for BAO fits to the monopole correlation function and isotropically averaged power spectrum, and anisotropic BAO fits and RSD fits to the monopole and quadrupole moments of the correlation function. These best-fitting strategies are dependent on the level of precision achieved within the covariance matrix. If more mocks were used, or higher precision could be achieved in some other way, then fits using more bins would become more desirable. However, after applying all corrections, the isotropically averaged BAO distance scale error recovered from the mocks is quite independent of bin size over a broad range of bin widths. This suggests that our best strategy will not change significantly even with better precision for the covariance matrix. The lack of sensitivity to bin size is good to see, as one would hope that the analysis method does not have a strong effect on the final measurements. The ability to recover the BAO scale without significant loss of accuracy using large bin sizes up to $12\,h^{-1}$ Mpc for $\xi(s)$ is perhaps more surprising, although we note that the BAO feature is quite broad.

Our analysis on bin sizes demonstrates that, on average, after correction, the recovered errors derived in multiple ways are a better match to each other than before correction. However, we caution that this match depends on the actual noise in the covariance matrix, which might be expected to be of the same order as the difference between correction factors. This match also relies on the model adopted being a good fit to the data. For the fit to BAO positions, it is clear that a poor model can yield incorrect likelihood errors, while leaving the distribution of best-fitting values relatively unaffected. The damping term in equation (24) is critical here – for any fit to data, if the model is overdamped, the likelihood maximum will be reduced as the model has more freedom to move, although the best-fitting location for each mock will generally not change by the same amount. For an underdamped model, the likelihood maximum will be increased, although the data themselves do not support such an apparent improvement in errors, as evidenced by the recovered distribution of best-fitting values. Further investigation is required, but is outside of the remit of this paper.

The comparison of BAO measurement errors as a function of bin size raises the interesting question of why the corrected error increases for increasing numbers of bins. The covariance matrix for large numbers of bins obviously still contains all the information used with a smaller number of bins, so theoretically you should be able to extract the same information from it and the data. As discussed in Section 1, the correct approach is to construct a joint likelihood of the data and mocks given the cosmological model to be tested. In the standard Gaussian assumption on the distributions of mocks and data, this is the same as that given by equation (5). Marginalizing over the true covariance matrix would then yield the final likelihood for the parameters given the mocks – in essence this should be the same for any bin choice for smooth models, where the binning results in minimal loss of information. The problem is that we are not performing this optimal likelihood approach if we assume that the estimated covariance matrix is 'correct' and use the standard likelihood equation (equation 1). In this approach, the effect of the covariance matrix, and the error it introduces through equation (1), changes with bin size: this dependence is given in equations (7) and (8), and is propagated through to the final error on the recovered parameters. Thus, the optimal bin size is actually only an optimal bin size if you want to retain equation (1) as the likelihood equation – in this case, the error does depend on bin size, and the error increases with increasing number of bins. The increase to large bin sizes can be more easily understood – here we are simply losing information as the averaging being performed increases in importance, leading to increasing errors. The minimum in the recovered error balances these two effects.

In Sections 6.5 and 6.6, we saw that the corrections required to the combined fits to both the monopole and quadrupole are quite large for both BAO and RSD measurements. This result suggests that there are significant gains to be obtained either by creating more accurate covariance matrices or by reworking the likelihood calculation to include covariance matrix errors. For future surveys, this effect will become increasingly important, and having too few

mocks or too poor a model for the covariance matrix will have a serious impact on the measurements made.

ACKNOWLEDGEMENTS

WJP acknowledges support from the UK Science & Technology Facilities Council (STFC) through the consolidated grant ST/K0090X/1 and from the European Research Council through the 'Starting Independent Research' grant 202686, MDEPUGS. AGS acknowledges support from the Trans-regional Collaborative Research Centre TR33 'The Dark Universe' of the German Research Foundation (DFG). Power spectrum calculations and fits made use of the COSMOS/Universe super-computer, a UK-Dirac facility supported by HEFCE and STFC in cooperation with CGI/Intel.

Funding for SDSS-III has been provided by the Alfred P. Sloan Foundation, the Participating Institutions, the National Science Foundation, and the US Department of Energy Office of Science. The SDSS-III website is http://www.sdss3.org/.

SDSS-III is managed by the Astrophysical Research Consortium for the Participating Institutions of the SDSS-III Collaboration including the University of Arizona, the Brazilian Participation Group, Brookhaven National Laboratory, University of Cambridge, Carnegie Mellon University, University of Florida, the French Participation Group, the German Participation Group, Harvard University, the Instituto de Astrofisica de Canarias, the Michigan State/Notre Dame/JINA Participation Group, Johns Hopkins University, Lawrence Berkeley National Laboratory, Max Planck Institute for Astrophysics, Max Planck Institute for Extraterrestrial Physics, New Mexico State University, New York University, Ohio State University, Pennsylvania State University, University of Portsmouth, Princeton University, the Spanish Participation Group, University of Tokyo, University of Utah, Vanderbilt University, University of Virginia, University of Washington, and Yale University.

REFERENCES

Ahn C. P. et al., 2012, ApJS, 203, 21
Ahn C. P. et al., 2013, ApJS, preprint (arXiv:1307.7735)
Anderson L. et al., 2012, MNRAS, 427, 3435
Anderson L. et al., 2013a, MNRAS, preprint (arXiv:1303.4666)
Anderson L. et al., 2013b, MNRAS, preprint (arXiv:1312.4877)
Berlind A. A., Weinberg D. H., 2002, ApJ, 575, 587
Beutler F. et al., 2013, MNRAS, preprint (arXiv:1312.4841)
Bolton A. et al., 2012, AJ, 144, 144
Chuang C.-H. et al., 2013, MNRAS, preprint (arXiv:1312.4889)
Cooray A., Sheth R., 2002, Phys. Rep., 372, 1
Davis M., Efstathiou G., Frenk C. S., White S. D. M., 1985, AJ, 292, 371
Dawson K. et al., 2013, AJ, 145, 10
Dodelson S., Schneider M. D., 2013, Phys. Rev. D., 88, 063537
Eisenstein D. J. et al., 2011, AJ, 142, 72
Gunn J. E. et al., 1998, AJ, 116, 3040
Gunn J. E. et al., 2006, AJ, 131, 2332
Hartlap J., Simon P., Schneider P., 2007, A&A, 464, 399
Kazin E. A. et al., 2013, MNRAS, 435, 64
Manera M. et al., 2013, MNRAS, 428, 1036
Manera M. et al., 2014, MNRAS, preprint (arXiv:1401.4171)
Peacock J. A., Smith R. E., 2000, MNRAS, 318, 1144
Planck Collaboration, 2013, A&A, preprint (arXiv:1303.5076)
Press S. J., 2005, Applied Multivariate Analysis, 2nd edn. Dover Press, New York
Reid B. A. et al., 2012, MNRAS, 426, 2719
Ross A. J. et al., 2013, MNRAS, 428, 1116
Ross A. et al., 2014, MNRAS, 437, 1109
Samushia L. et al., 2013, MNRAS, preprint (arXiv:1312.4899)
Sanchez A. et al., 2013, MNRAS, preprint (arXiv:1312.4854)
Smee S. A. et al., 2013, AJ, 126, 32
Taylor A., Joachimi B., Kitching T., 2012, MNRAS, 432, 1928
Tojeiro R. et al., 2014, MNRAS, preprint (arXiv:1401.1768)

This paper has been typeset from a TEX/LATEX file prepared by the author.